The 2010 Michael W. O'Neill Lecture
Proceedings, CIGMAT - University of Houston – 23 April 2010

EVALUATING EXCAVATION SUPPORT SYSTEMS TO PROTECT ADJACENT STRUCTURES

Richard J. Finno
Dep't. of Civil and Environmental Engrg., Northwestern University
2145 Sheridan Road, Evanston, IL 60208
Email: r-finno@northwestern.edu

ABSTRACT This paper presents an overview of methods that can be used to predict damage to buildings as a result of excavation-induced ground movements and describes an adaptive management approach for predicting, monitoring, and controlling excavation-induced ground movements. Successful updating of performance predictions depends equally on reasonable numerical simulations of performance, the type of monitoring data used as observations, and the optimization techniques used to minimize the difference between predictions and observed performance. This paper summarizes each of these factors and emphasizes their inter-dependence. Applications of these techniques from case studies are presented to illustrate the capabilities of this approach. Examples are given to show how optimized parameter based on data obtained at early stages of excavation can be used to predict performance at latter stages, and how these optimized parameters can be applied to other excavations in similar geologic conditions.

INTRODUCTION

Damage to buildings adjacent to excavations can be a major design consideration when constructing facilities in congested urban areas. As new buildings are constructed, the excavations required for basements affect nearby existing buildings, especially those founded on shallow foundations. Often excavation support system design must prevent any damage to adjacent structures or balance the cost of a stiffer support system with the cost of repairing damage to the affected structures. In either case, it is necessary to predict the ground movements that will induce damage to a structure. Practically speaking, a designer is attempting to limit/prevent damage to either the architectural details of a building, which occurs prior to structural damage, or to load bearing walls.

To evaluate damage potential in buildings affected by ground movements resulting from deep excavations, one must first predict the magnitude and distribution of ground movements caused by the excavation. This may be done using empirical or finite element methods, depending on the importance of the building, budget considerations, and design phase of the investigation. After locating the affected building in relation to the expected ground movements, one then evaluates the impact of these movements on the building. The main two sources of uncertainties in this analysis are the structural evaluation of the affected building and the movement prediction. This paper summarizes damage evaluation methods and describes an adaptive management approach for predicting, monitoring and controlling ground movements. This approach can be thought of as an "automated" observational approach (Peck 1969). This methodology is a useful design tool in that decisions regarding trigger levels and responses can be thoroughly evaluated during design.

CRITERIA TO EVALUATE EXCAVATION-INDUCED DAMAGE

Selected criteria that are applicable to evaluate excavation-induced damage are summarized in Table 1, wherein the relevant parameter and its limiting value are shown. Note that the parameter used to relate structural movements at the foundation level to damage depends on the method. Deep beam methods are more general than empirical methods (e.g., Skempton and McDonald 1956) which are applicable to damage of structures based on settlements arising from the weight of the structure.

Table 1. Selected damage criteria for excavation-induced damage to buildings

Reference	Type of method	Limiting parameter	Applicability
Burland and Wroth (1975)	Deep beam model of building	$\Delta /(L\ \varepsilon_{crit})$	Load bearing wall (E/G = 2.6), framed structures (E/G = 12.5), and masonry building (E/G = 0.5) with no lateral strain
Boscardin and Cording (1989)	Extended deep beam model	β, ε_h	L/H = 1 and assumption horizontal ground and building strains are equal
Son and Cording (2005)	Semi-empirical	Average strain	Masonry structures; need relative soil/structure stiffness; use average strain in distorting part of structure
Finno et al (2005)	Laminate beam model	$\Delta /(L\ \varepsilon_{crit})$	Load bearing walls, framed structures, masonry buildings, need bending and shear stiffness of components of walls and floors
Boone (1996)	Detailed analysis of structure	crack width	general procedure that considers bending and shear stiffness of building sections, distribution of ground movements, slip between foundation and grade and building configuration

The following terms are related to the limiting parameters in Table 1, and are illustrated in Figure 1. Differential settlement between two points, *i* and *j*, is δ_{ij}. The distance between two points i and j is ℓ_{ij}. Distortion between two points, *i* and *j*, is defined as δ_{ij}/ℓ_{ij}. A concave-up deformation is commonly called "sagging," while a concave-down deformation is termed "hogging." An inflection point separates two modes of deformation. The length of a particular mode of deformation, bounded by either the ends of a building or inflection points of the settlement profile, is L. The average slope, *m*, of a specific mode of deformation is defined as δ_{kl}/L_{kl}, where the subscripts *k* and *l* are boundaries of the mode of deformation. This slope differs from the distortion, δ_{ij}/ℓ_{ij}, which is the ratio for two adjacent points. The relative settlement of each mode, Δ, is the maximum deviation from the average slope of a particular deformation mode. The deflection ratio, Δ/L, is the ratio of the relative settlement to the length of the deflected part. Rigid body rotation of the building, ω, is the tilt of the building and causes no stresses or strains in the building. Angular distortion, β_{ij}, is the difference between distortion, δ_{ij}/ℓ_{ij}, and rigid body rotation, ω.

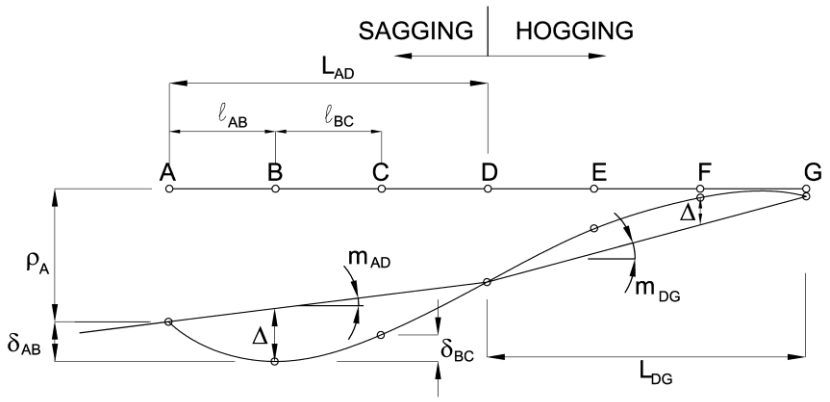

Figure 1. Quantities used to define limiting parameters for damage criteria

The critical tensile strain, $\varepsilon_{crit.}$, is that at which cracking becomes evident. Tensile strains, ε_t, can be caused by bending, ε_b, diagonal tension due to shear, ε_d , or horizontal extension, ε_h, caused by lateral extension of the building due to lateral movement in the soil mass below the footings. Critical strains that cause failure in common building materials vary widely as a function of material and mode of deformation (Boone 1996).

Burland and Wroth (1975) modeled a building as a deep isotropic beam to relate strains in the building to the imposed deformations, as illustrated in Figure 2. They suggested that for the sagging type deformations shown in the figure, the neutral axis is located at the middle of the beam. For hogging type deformations, they assumed the foundation and soil provide significant restraint to deformations, effectively moving the neutral axis to its bottom. They presented equations for limiting Δ/L in terms of maximum bending strain and maximum diagonal tensile strain for a linear elastic beam with a Poisson's ratio, ν, of 0.3 (implying a Young's modulus/shear modulus ratio, E/G, of 2.6) subjected to a point load with the neutral axis at either the center or bottom of the beam. A building not adequately represented by an isotropic elastic beam is characterized by different E/G ratios. They postulated that for buildings with significant tensile restraint, or very flexible in shear (i.e. frame buildings), an E/G ratio of 12.5 would be appropriate. However, for buildings that have little or no tensile restraint (i.e. traditional masonry buildings), they recommended that the E/G ratio should be 0.5.

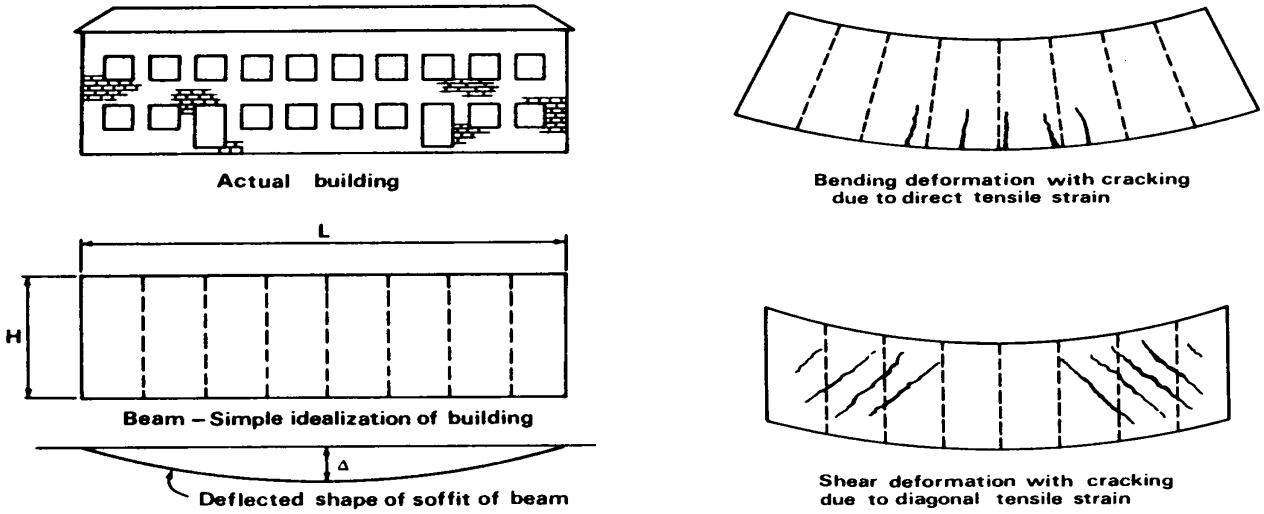

Figure 2. Deep beam idealization of building (after Burland and Wroth 1975)

Boscardin and Cording (1989) extended this deep beam model to include horizontal extension strains, ε_h, caused by lateral ground movements. They presented a chart relating β and ε_h to levels of damage for buildings with brick, load-bearing walls and an L/H ratio of 1 undergoing a hogging deformation with the neutral axis at the bottom. Similar to Burland and Wroth (1975), the building is idealized as a linear elastic beam with υ equal to 0.3. Direct transfer of horizontal ground strain to the structure is assumed in this approach, which may or may not be reasonable depending on the structure. For example, modern frame structures with floors that act as diaphragms do not move laterally with the ground (e.g. Geddes 1977,1991; Finno et al. 2002) for deformations normally associated with adjacent excavations.

Son and Cording (2005) extended the Boscardin and Cording approach in a semi-empirical manner. Resulting criteria are applicable to masonry buildings. They proposed use of a damage criterion based on the average state of strain within the distorting portion of a building. Their revised criterion is independent of E/G, L/H and the position of the neutral axis of the wall. They explicitly considered the shear stiffness of the walls on the distortions imposed by the ground settlements. They used model test and results of numerical simulations as well as case studies of building damage and distortion to calibrate the model. They noted that cracking in masonry walls significantly reduced effective wall stiffness. There is considerable overlap in categories of damage as a function of their parameters.

Finno et al. (2005) extended the Burland and Wroth (1975) equations to allow explicit input of E/G and location of the neutral axis, resulting in equations that relate limiting Δ/L to bending strain at the top, $\varepsilon_{b(top)}$, and bottom of a beam, $\varepsilon_{b(bottom)}$, and the maximum diagonal tensile strain, $\varepsilon_{d(average)}$. Figure 3 shows the effects of different E/G ratios on the conditions required for initial cracking. The kink in a curve represents the limit between shear critical and bending critical geometries of a beam. These results show that the limiting deflection ratio that causes cracks varies over wide limits, implying that structural details of a building must be considered when establishing criteria. However, it is difficult to select the beam characteristic parameter E/G and the neutral axis location when developing a deep beam model for many structures, i.e., multi-story structures.

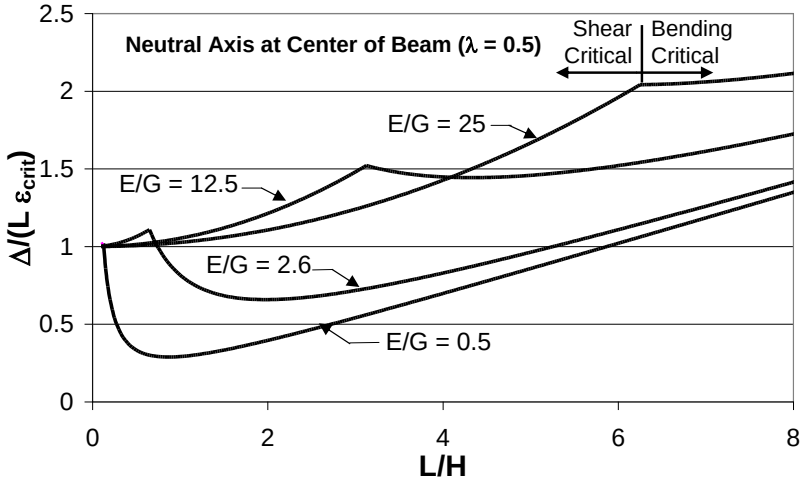

Figure 3. Effect of E/G on critical tensile strain (from Finno et al. 2005)

To provide a more realistic model of a structure and yet maintain relative simplicity, Finno et al (2005) proposed a laminate beam model to represent the response of a building to

imposed deformations. Burland and Wroth (1975) modeled a building as a rectangular beam with unit thickness, which implicitly assumes a constant value of I/A_v for the building. In the laminate beam approach, the parameter EI/GA_v accounts for variations in bending and shear stiffness of a structure. This reflects the fact that bending is proportional to the bending stiffness, EI, where I is the moment of inertia of the beam, whereas deformation due to shear is proportional to the shear modulus times the area contributing to shear resistance, GA_v. The laminate beam model assumes that the floors offer restraint to bending deformations, and the walls, whether load bearing or infill between columns, offer restraint to shear deformations. These parameters can be explicitly considered for each floor and wall system in a multi-story building. See Finno et al (2005) for more details.

Boone (1996) presented a more detailed approach to evaluate building damage due to differential ground movement caused by adjacent construction. This method considers structure geometry and design, strain superposition and critical strains of building materials. Load bearing walls are modeled as uniformly-loaded, simple-supported beams. Damage to frame buildings is assumed to occur from differential vertical movements of columns, depending on the column's tilt and degree of fixity. Damage to infill walls is presumed to occur as a result of the deformed shape of the surrounding beams and columns. If a structure is subjected to horizontal extension, then these strains are superposed on the ones caused by bending and shear.

None of these models has been developed consider the strains that occur when the building settles under its own weight. Conceptually, one could estimate the residual strains and superpose them upon those arising during excavation. However, defining how much settlement would have occurred prior to attaching in-fill walls to a structural frame during the original building construction would be a difficult task. The movements to which these architectural portions of the structure would have been subjected are less than the total settlements. Furthermore, the author is unaware of any performance data that includes both self-weight and excavation-induced movements. In any case, this aspect of response warrants further study.

The variability of the magnitude of movements that cause damage to the architectural details, as illustrated in Figure 3 suggests that either a conservative approach or a detailed structural analysis of an affected building is warranted when establishing allowable movements for an excavation. If possible, the owners of the affected buildings should be kept informed of the planned operations. Because at times it becomes very expensive to construct a stiff enough system to prevent all damage, the optimal solution may be one where a repair cost for inevitable minor architectural damage is included in the bid package, after, of course, securing the cooperation of the building's owner.

ADAPTIVE MANAGEMENT APPROACH

Once limiting movement criteria have been established, an adaptive management approach can be employed to predict, monitor and control ground movements during excavation. This approach is summarized in Figure 4. The left hand column represents calculations made during the design and updating phases, and includes finite element computations. Inclinometer, optical survey and strain gage data have been collected at sites and used as observations against the predictions are compared. The center column is the optimization needed to update predictions based on the measurements. Ideally, this process works automatically, all data collected in the field is transferred in real time to a host computer where it can be processed into format compatible with the numerical analyses. After data are collected at early stages of an

excavation, updated parameters form the basis of a new simulation to predict responses at later, and presumably more critical, stages of excavations.

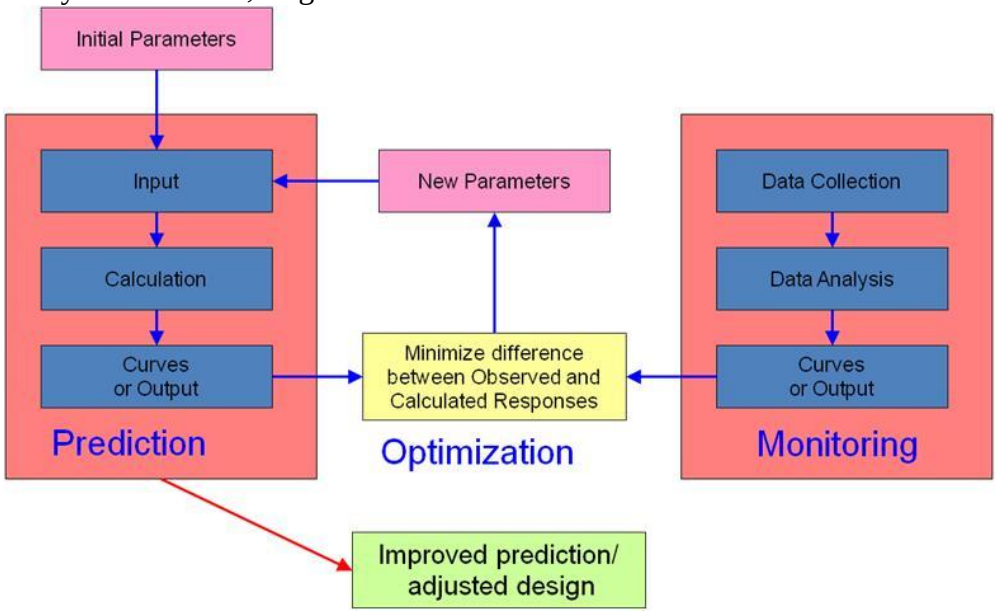

Figure 4. Adaptive management approach

Successful use of this approach depends equally on reasonable numerical simulations of performance, the type of monitoring data used as observations, and the optimization techniques used to minimize the difference between predictions and observed performance. This section summarizes each of these factors and emphasizes their inter-dependence. Numerical considerations are described, including the initial stress and boundary conditions, the importance of reasonable representation of the construction process, and factors affecting the selection of the constitutive model. Monitoring data that can be used in conjunction with current numerical capabilities are discussed. Self-updating numerical models that have been successfully used to compute anticipated ground movements, update predictions of field observations and to learn from field observations are summarized. Applications of these techniques from case studies are presented to illustrate the capabilities of this approach.

Numerical simulations

While supported excavations commonly are simulated numerically by modeling stages of excavation and support installation, it is necessary to simulate all aspects of the construction process that affect the stress conditions around the excavation to obtain an accurate prediction of behavior. This may involve simulating previous construction activities at the site, installation of the supporting wall and any deep foundation elements, as well as the removal of cross-lot supports or detensioning of tiedback ground anchors. Furthermore, issues of time effects caused by hydrodynamic effects or material responses may be important.

Finno and Tu (2006) summarized the effects of a number of key numerical assumptions on the computed performance of supported excavations. The manner in which the excavation is simulated including the removal of soil elements in a finite elements mesh should satisfy the principal of superposition as described by Ghaboussi and Pecknold (1985). Other key assumptions include selecting appropriate drainage conditions during excavation (Clough and Mana 1976; O'Rourke and O'Donnell 1997; Whittle et al. 1993), starting with appropriate initial

effective stresses that include the effects of past construction activities at a site (Calvello and Finno 2003), and accurately defining the initial ground water conditions for a site (e.g. Finno et al. 1988). Many times the effects of the installation of a wall are ignored in a finite element simulation and the wall is "wished-into-place" with no change in the stress conditions in the ground or any attendant ground movements. However, there is abundant information (e.g. Clough et al. 1989; O'Rourke and Clough 1990; Finno et al. 1988; Sabatini 1991; Koutsoftas et al. 2000) that shows ground movements may arise during installation of the wall, and, if ignored, these may have a significant impact on the accuracy of the computed responses, particularly in cases where the resulting ground deformations are relatively small. One also must take care when representing the bracing system in a model. In typical plane strain simulations, application of prestress for cross-lot braces and installation of tiedback ground anchors can present problems under certain circumstances (e.g. Finno and Tu 2006).

Even with properly defined initial conditions, challenges remain. Excavation and support installation normally occur under conditions that are three dimensional. If one is making a computation assuming plane strain conditions, then one must judiciously select a data set so that planar conditions are applicable to a set of inclinometer data. If one is using an adaptive management approach wherein data is collected and compared with numerical predictions in almost real time, then it is clear that a 3D analysis would be required for most days as a result of the uneven excavated surface and timing of the anchor prestressing operations.

Even when a sufficiently extensive horizontal excavated surface is identified, 3-dimensional effects may still arise from the higher stiffness at the corners of an excavation. These boundary conditions lead to smaller ground movements near the corners and larger ground movements towards the middle of the excavation wall (Ou et al. 1996; Finno et al. 2007). Another, and less recognized, consequence of the corner stiffening effects is the maximum movement near the center of an excavation wall may not correspond to that found from a conventional plane strain simulation of the excavation, i.e., 3-dimensional (3-D) and plane strain simulations of the excavation do not yield the same movement at the center portion of the excavation, even if the movements in the center are perpendicular to the wall. This effect can be quantified by the plane strain ratio, PSR, defined as the maximum movement in the center of an excavation wall computed by 3-D analyses divided by that computed by a plane strain simulation. As shown in Figure 5, a key indicator is the L/H_e ratio, where L is the dimension of the excavation where the movement occurs, and H_e is the excavation depth. When L/H_e is greater than 6, the PSR is equal to 1 and results of plane strain simulations yield the same displacements in the center of an excavation as those computed by a 3-D simulation. When L/H_e is less than 6, the displacement computed from the results of a plane strain analysis will be larger than that from a 3-D analysis. When conducting an inverse analysis of an excavation with a plane strain simulation, the effects of this corner stiffening is that an optimized stiffness parameter will be larger than it really is because of the lack of the corner stiffening in the plane strain analysis. This effect becomes greater as an excavation is deepened because the L/H_e value decreases as the excavated grade is lowered. This trend was observed in the optimized parameters for the deeper strata at the Chicago-State subway renovation excavation (Finno and Calvello 2005).

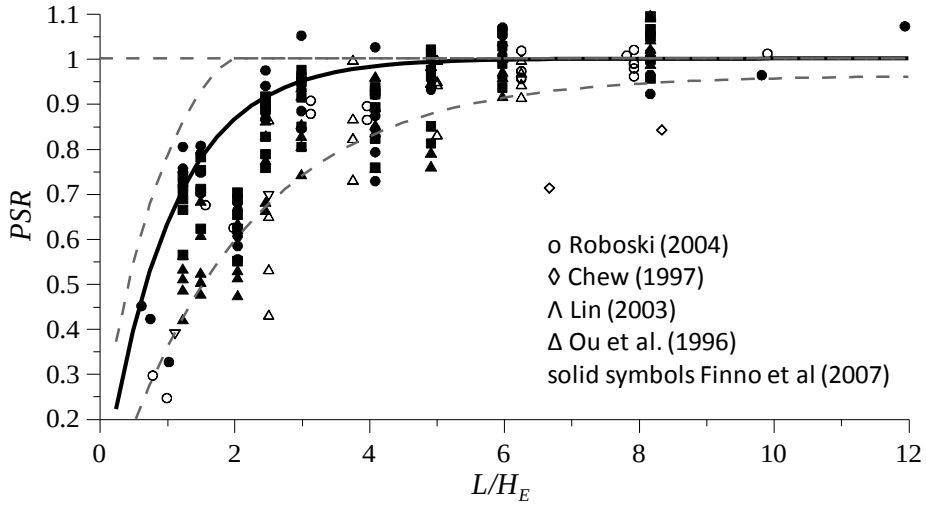

Figure 5. Effects of geometry on 3-D movements of excavations

Soil Constitutive Behavior

When one undertakes a numerical simulation of a deep supported excavation, one of the key decisions made early in the process is the selection of the material constitutive models representing the various soil formations at the site. If the results form the basis of a prediction that will be updated based on field performance data, then the types of field data that form the basis of the comparison will impact the applicability of a particular model. Possibilities include lateral movements based on inclinometers, vertical movements at various depths and distances from an excavation wall and/or forces in structural support elements. When used for a case where control of ground movements is a key design consideration, the constitutive model must be able to reproduce the soil response at appropriate strain levels to the imposed loadings.

It is useful to recognize that soil is an incrementally nonlinear material, i.e., its stiffness depends on loading direction and strain level. Soils are neither linear elastic nor elasto-plastic, but exhibit complex behavior characterized by zones of high constant stiffness at very small strains, followed by decreasing stiffness with increasing strain. This behavior under static loading initially was realized through back-analysis of foundation and excavation movements in the United Kingdom (Burland, 1989). The recognition of zones of high initial stiffness under typical field conditions was followed by efforts to measure this ubiquitous behavior in the laboratory for various types of soil (Jardine et al, 1984; Clayton and Heymann 2001; Santagata et al. 2005; Callisto and Calebresi 1998, Holman 2005, Cho and Finno 2010). Furthermore, the stiffness depends on the direction of loading as measured from the most recently applied stress path, or recent stress history.

To illustrate small strain nonlinearity and recent stress history effects on shear stiffness for Chicago clays, secant shear modulus from drained constant mean normal stress (CMS) and constant mean normal stress extension (CMSE) stress paths are plotted versus shear strains in Figure 6. These specimens with an OCR of 1.7 were obtained from block samples cut from an excavation in Evanston, IL (Blackburn and Finno 2007). In all cases, the secant shear modulus at 0.1% strain, the smallest strain reliably measured in conventional triaxial equipment, was about 4 to 8 times less than that measured at 0.002% strain, the smallest value obtained with the internal instrumentation used in these experiments. Complete details and results of the testing program are presented by Cho (2007).

In Figure 6, the angles noted next to the stress paths are calculated as the absolute value of the angle change from the previous stress path ($\theta = 0°$). The results of the two "K_0" probe tests showed dependence on the angle change, with the CMSE path (unloading) exhibiting a stiffer response than that of the CME (loading type). For the "post-unloading" probe tests, with a recent stress history representative of a site where an old building with a basement was demolished before excavation, the opposite directional dependency is observed. The stiffness of loading path (U-CMS) is much greater than those of unloading path (U-CMSE). Interestingly, shear moduli magnitudes in the loading path (K_0-CMS) of the "K_0" probes and the unloading path (U-CMSE) of the "post-unloading" probes with similar values of θ are quite alike, even though the current stress path direction is exactly the opposite. Considering the change in θ, as shown in the inset of Figure 6, the stiffer shear moduli occur at the stress path corresponding to nearly complete stress reversals, U-CMS (θ =160°) and K_0-CMSE (θ =147°). Although the data are limited, it shows the effects of recent stress history on the shear stiffness. Also, little difference was noted at strains larger than 0.1%, as reported by Atkinson et al (1990). Thus is appears that recent stress history effects are significant for these clays – G_{sec} at about 0.002% strain varies by a factor of 2.

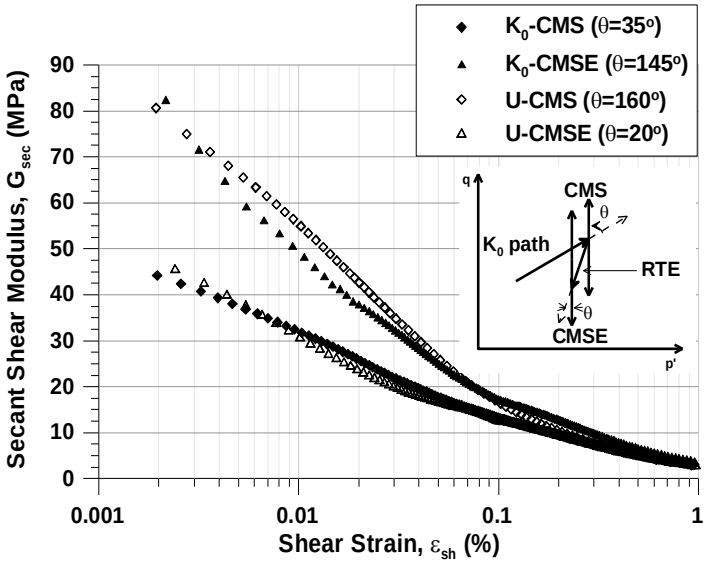

Figure 6. Recent stress history effects on secant shear modulus: Chicago glacial clay (Cho and Finno 2010)

Burland (1989) suggested that working strain levels in soil around well-designed tunnels and foundations are on the order of 0.1 %. If one uses data collected with conventional triaxial equipment to discern the soil responses in many practical situations, it is not possible to accurately incorporate site-specific small strain non-linearity into a constitutive model based on conventionally-derived laboratory data. There are a number of models reported in literature wherein the variation of small strain nonlinearity can be represented, for example, a three-surface kinematic model develop for stiff London clay (Stallebrass and Taylor 1997), MIT-E3 (Whittle and Kavvadas 1994), hypoplasticity models (e.g. Viggiani and Tamagnini 1999), and a directional stiffness model (Tu 2007). These models require either detailed experimental results or experience with the model in a given geology to derive parameters. More work is needed to relate these actual soil responses to conventionally-obtained field and laboratory data to incorporate these responses into practice.

For most current practical applications, one uses simpler, elasto-plastic models contained in material libraries in commercial codes. For these models, a key decision is to select the elastic parameters that are representative of the secant values that correspond to the predominant strain levels in the soil mass. Examples of the strain levels behind a wall for an excavation with lateral wall movements of 29 and, 57 mm are shown in Figure 7. These strain levels were computed based on the results of displacement-controlled simulations where the lateral wall movements and surface settlements were incrementally applied to the boundaries of a finite element mesh. The patterns of movements were typical of excavations through clays, and were based on those observed at an excavation made through Chicago clays (Finno and Blackburn 2005). Because the simulations were displacement-controlled, the computed strains do not depend on the assumed constitutive behavior.

As can be seen in Figure 7, the maximum shear strains correspond to about 0.3% for 29 mm maximum wall lateral movement, and represent good control of ground movements in these soft soils. Shear strains as high as 0.7% occurred when 57 mm of maximum wall movement develop. These strain levels can be accurately measured in conventional triaxial testing, and thus if one can obtain specimens of sufficiently high quality, then secant moduli corresponding to these strain levels can be determined via conventional laboratory testing. Because the maximum horizontal wall displacement can be thought of as a summation of the horizontal strains behind a wall, the maximum wall movements can be accurately calculated with a selection of elastic parameters that correspond to these expected strain levels. The fact that small strain non-linearity is not explicitly considered will not have a large impact on the computed horizontal wall displacements because they are dominated by the larger strains in the soil mass. Consequently, these computed movements would be compatible with those measured by an inclinometer located close to the wall.

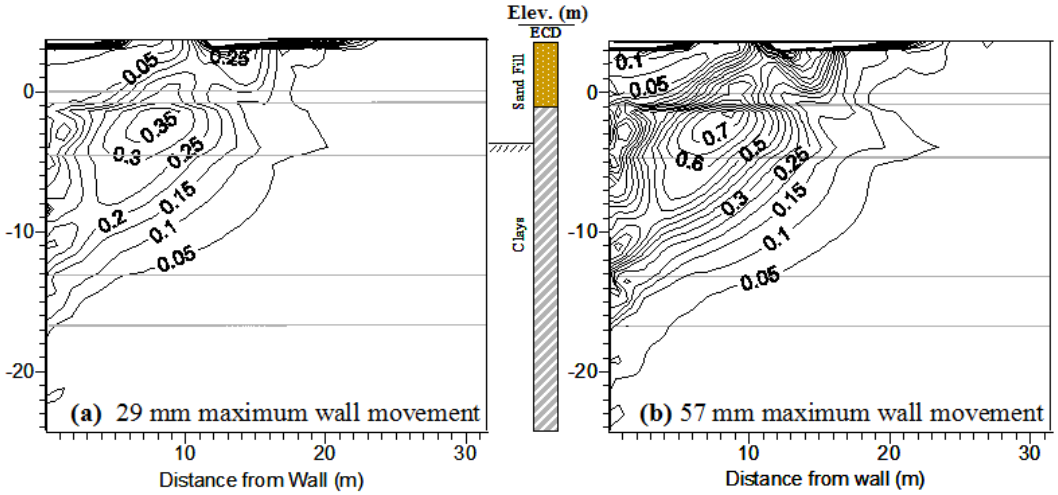

Figure 7. Shear strain levels behind excavation (contours in %)

However, if one needs to have an accurate representation of the distribution of ground movements with distance from the wall, then this approach of selecting strain-level appropriate elastic parameters will not work. The small strain non-linearity must be explicitly considered to find the extent of the settlement because the strains in the area of interest vary from the maximum value to zero. As a consequence, many cases reported in literature indicate computed wall movements agree reasonably well with observed values, but the results from the same computations do not accurately reflect the distribution of settlements. Good agreement at

distances away from a wall can be obtained only if the small stain non-linearity and dilation responses, if appropriate, of the soil are adequately represented in the constitutive model.

Self-updating Models

Self-updating models can be of two types, one wherein the constitutive responses are assumed and key parameters of the model are updated using inverse techniques based on selected field observations, and the other wherein the field observations are used to define the constitutive response using artificial neural nets (Hashash et al. 2006). Herein, an inverse technique based on a gradient method (e.g., Ou and Tang 1994; Ledesma et al., 1996; Calvello and Finno 2004) is applied. The method employs local parameter identification of a specific constitutive law. The gradient method described herein uses UCODE (Poeter and Hill, 1998), a computer code designed to allow inverse modeling posed as a parameter estimation problem. Macros were written in a windows environment to couple UCODE with PLAXIS, a commercial finite element code. Alternatively, the approach can be implemented by using the optimization routines in the MATLAB toolbox.

Figure 8 shows a flowchart of a parameter optimization algorithm appropriate for a gradient method. With the results of a finite element prediction in hand, the computed results are compared with field observations in terms of weighted least-squares objective function, S($\underline{b}$):

$$S(\underline{b}) = \left[\underline{y} - \underline{y}'(\underline{b})\right]^T \underline{\omega}\left[\underline{y} - \underline{y}'(\underline{b})\right] = \underline{e}^T \underline{\omega}\underline{e} \tag{1}$$

where $\underline{b}$ is a vector containing values of the parameters to be estimated; $\underline{y}$ is the vector of the observations being matched by the regression; $\underline{y}'(\underline{b})$ is the vector of the computed values which correspond to observations; $\underline{\omega}$ is the weight matrix wherein the weight of every observation is taken as the inverse of its error variance; and $\underline{e}$ is the vector of residuals. This function represents a quantitative measure of the accuracy of the predictions.

A sensitivity matrix, $\underline{X}$, is then computed using a forward difference approximation based on the changes in the computed solution due to slight perturbations of the estimated parameter values. This step requires multiple runs of the finite element code. Regression analysis of this non-linear problem is used to find the values of the parameters that result in a best fit between the computed and observed values. This fitting can be accomplished with the modified Gauss-Newton method, the results of which allow the parameters to be updated using:

$$\left(\underline{C}^T \underline{X}_r^T \omega \underline{X}_r \underline{C} + \underline{I}\, m_r\right)\underline{C}^{-1}\underline{d}_r = \underline{C}^T \underline{X}_r^T \omega\left(\underline{y} - \underline{y}'(\underline{b}_r)\right) \tag{2}$$

$$\underline{b}_{r+1} = \rho_r \underline{d}_r + \underline{b}_r \tag{3}$$

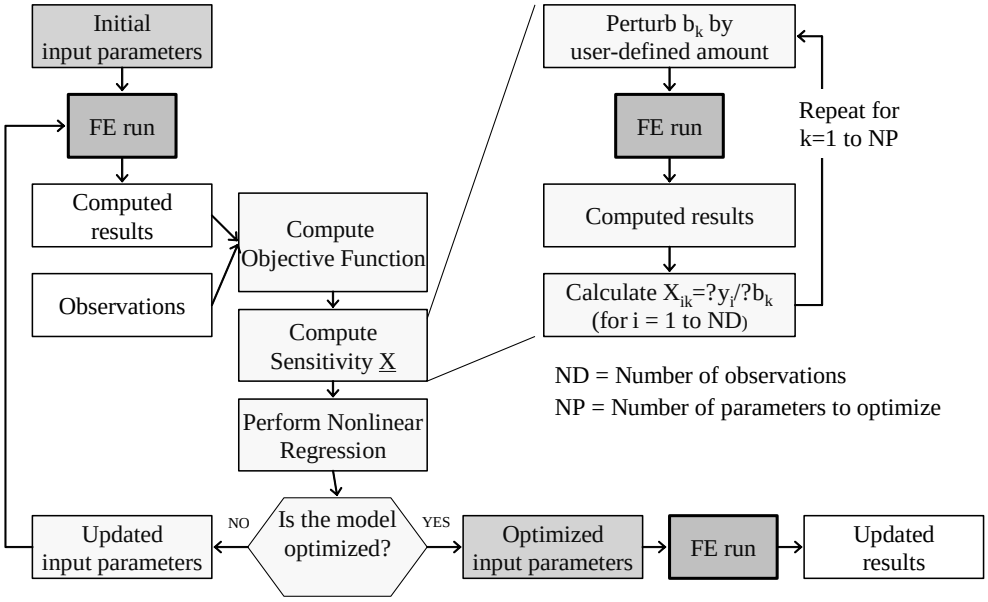

Figure 8. Flow chart for gradient method

where d_r is the vector used to update the parameter estimates b; r is the parameter estimation iteration number; X_r is the sensitivity matrix ($X_{ij}=\partial y_i/\partial b_j$) evaluated at parameter estimate $\underline{b}_r$; $\underline{C}$ is a diagonal scaling matrix with elements c_{jj} equal to $1/\sqrt{(\underline{X}^T \underline{\omega}\ \underline{X})_{jj}}$; $\underline{I}$ is the identity matrix; m_r is the Marquardt parameter used to improve regression performance; and $\underline{d}_r$ is a damping parameter, computed as the change in consecutive estimates of a parameter normalized by its initial value, but is restricted to values less than 0.5.

At a given iteration, after performing the modified Gauss-Newton optimization, the updated model is considered optimized if either of two convergence criteria is met: (i) the maximum parameter change of a given iteration is less than a user-defined percentage of the value of the parameter at the previous iteration; (ii) the objective function, S($\underline{b}$), changes less than a user-defined amount for three consecutive iterations. After the model is optimized, the final set of input parameters is used to run the finite element model one last time and produce the "updated" prediction of future performance. See Rechea (2006) for details concerning the convergence criteria as applied to excavations.

The weight of an observation can be expressed as the inverse of the variance for the 95% confidence interval for the accuracy of a measurement:

$$weight = \frac{1}{\sigma^2} \qquad \sigma = \frac{Accuracy}{1.96} \tag{4}$$

In this way, more reliable data (smaller variability) are given greater emphasis. The errors associated to measurements are usually related to the accuracy of the instrumentation, and independent of the magnitude of the observation (assuming the observation is within the range of the instrumentation). Table 2 shows how to obtain weights for various types of instrumentation. Accuracies and ranges in Table 2 are taken from manufacturer's literature, and are meant to be representative of typical values in the field. Smaller values can be used based on field data

collected prior to any activity at the site, assuming enough data are collected to adequately define the variation about the initial value (Langousis 2007).

Table 2: Typical weights of observations

Instrumentation	Range (full scale)	Accuracy	95% standard deviation, σ	Weight
Lateral movements with inclinometers	± 53° from Vertical	± 0.25 mm/m $\frac{0.25}{1000}\cdot d$	$\frac{0.25}{1000}\cdot\frac{d}{1.96}=0.0001\cdot d$ (m)	$\frac{1}{(0.0001\cdot d)^2}$
		where *d* is distance (m) from bottom of casing		
Ground surface settlement with optical survey		± 0.01 ft ± 0.003 m	$\frac{0.003}{1.96}=0.00155$ (m)	$\frac{1}{(0.00155)^2}$
vibrating wire piezometer	3.5 bar/50 psi 344.8 Pa	± 0.1% FS ± 0.34 Pa	$\frac{0.34}{1.96}=0.173$ (Pa)	$\frac{1}{(0.173)^2}$
Strut force with spot-weldable strain gauge	2,500 microstrain	± 0.1%FS = ± 2.5 microstrain	$\frac{E\cdot A\cdot Accuracy}{1.96}$ (kN)	$\frac{1}{(6.19)^2}$ (1)

(1) value shown is for a steel brace with A = 0.024 m^2

Inverse analysis algorithms allow the simultaneous calibration of multiple input parameters. However, identifying the important parameters to include in the inverse analysis can be problematic, and it is not possible to use a regression analysis to estimate every input parameter of a given excavation simulation. The relative importance of the input parameters being simultaneously estimated can be defined using various parameter statistics (Hill 1998). The statistics found useful for this type of work are the composite scaled sensitivity, ccs_j, and the correlation coefficient, *cor(i,j)*. The value of css_j indicates the total amount of information provided by the observations for the estimation of parameter j, and is defined as:

$$css_j = \left[\sum_{j=1}^{ND}\left(\left(\frac{\partial y'_i}{\partial b_j}\right)b_j\omega_{ii}^{1/2}\right)^2\Bigg|_{\underline{b}}\Big/ND\right]^{1/2} \tag{5}$$

where y'_i is the i^{th} computed value, b_j is the j^{th} estimated parameter, $\partial y_i/\partial b_j$ is the sensitivity of the i^{th} computed value with respect to the j^{th} parameter, ω_{jj} is the weight of the i^{th} observation, and ND is the number of observations.

The values of the matrix *cor (i,j)* indicate the correlation between the i^{th} and j^{th} parameters, and are defined as:

$$cor(i,j)=\frac{\mathrm{cov}(i,j)}{\mathrm{var}(i)^{1/2}\,\mathrm{var}(j)^{1/2}} \tag{6}$$

where cov(*i*,*j*) equal the off-diagonal elements of the variance-covariance matrix $\underline{V}(\underline{b}')=s^2(\underline{X}^T\underline{\omega}\underline{X})^{-1}$, and var(*i*) and var(*j*) refer to the diagonal elements of $\underline{V}(\underline{b}')$.

The number and type of input parameters that one can expect to estimate simultaneously depend on a number of factors, including the soil models used, the stress conditions of the simulated system, available observations, and numerical implementation issues. Examples of this procedure are presented by Calvello and Finno (2004) and Finno and Calvello (2005).

Monitoring

The assumptions inherent in any prediction limit the types of data that can be used as a basis of updating performance predictions. Consequently, one must carefully select the types of data, location of the measuring points, and the excavation conditions when applying an inverse technique . Inclinometer data based on measurements close to a support wall are the most useful when typical elasto-plastic constitutive models are assumed to represent soil behavior, as is the case when employing commercial finite element codes, for reasons discussed in the last section. These data can be supplemented by ground surface settlements when using a constitutive model that accounts for small strain nonlinearities and dilation (Finno and Tu 2006, Hashash and Whittle, 1996). Furthermore, other types of measurements, such as forces in internal braces and pore water pressures, conceptually can be used in conjunction with displacement measurements to make the computed results more sensitive to parameters selected for optimization (Rechea 2006). However, if the bracing forces are used in the analyses, then either they must be corrected for the effects of temperature or the numerical simulation must explicitly include the temperature induced changes in the support system. This latter feature is not normally included in commercial finite element codes.

While these different types of data can be handled within a properly formulated inverse analysis, the timely collection and screening of the data must be successfully accomplished (Finno 2007). Furthermore, for any monitoring system to be fully automated, one must be able to track construction progress so that performance data can be correlated with the excavation activities. To correlate the numerical data with the causative actions of the excavation process, imaging technologies can be employed to provide an accurate and detailed record of construction activities. Trupp et al. (2004) and Su et a. (2006) used 3-D laser scanning to capture an accurate image of the geometry of the excavation to provide an accurate, as-built digital record of construction. Sections may be taken from these scans and imported into a finite element code to provide an accurate excavation surface for input to inverse analysis. An internet accessible weather-resistant video camera has been used on several projects to allow remote visualization of the construction process in real-time, as well as a dated, photographic record of construction (Finno and Blackburn 2005). Significant developments have been made in automated systems to continuously monitor deformations due to construction activities. These systems provide the engineer with uninterrupted stream of data in near real time without the need to wait for manual data readings. Such systems are essential tools for making timely decisions regarding changes in construction activities and support installation to mitigate potential damage to adjacent facilities. However, real-time, completely automated updating is not yet possible, although updated paratmeres can be obtained within 8 hours after field data has been acquired.

CAPABILITIES OF THE ADAPTIVE MANAGEMENT METHOD

Examples of the gradient method applied to supported excavations are presented to illustrate (i) its ability to identify optimized parameters based on observations made during early stages of excavation so as to allow accurate predictions of performance of latter stages of an

excavation, and, (ii) the applicability of optimized parameters found based on performance data of one excavation to others in the same geology.

The finite element software PLAXIS was used to compute the plane strain response of the soil around these excavations. The hardening-soil model (H-S) (Schanz et al. 1999) was assumed to represent soil responses for these examples. Parameters from other constitutive models have been optimized as well (e.g., Calvello and Finno 2002).

The effective stress H-S model is formulated within the framework of elasto-plasticity. Plastic strains are calculated assuming multi-surface yield criteria. Isotropic hardening is assumed for both shear and volumetric strains. The flow rule is non-associative for frictional shear hardening and associative for the volumetric cap. Six basic H-S input parameters define the constitutive soil responses, the friction angle, φ, cohesion, c, dilation angle, ψ, the reference secant Young's modulus at the 50% stress level, E_{50}^{ref}, the reference oedometer tangent modulus, E_{oed}^{ref}, and the exponent *m* which relates reference moduli to the stress level dependent moduli (E representing E_{50}, E_{oed}, and E_{ur}):

$$E = E^{ref}\left(\frac{c\cot\phi - \sigma_3^{'}}{c\cot\phi + p^{ref}}\right)^{m} \tag{7}$$

where p^{ref} is a reference pressure equal to 100 stress units and σ'_3 is the minor principal effective stress. A sensitivity analysis indicated that the model's relevant and uncorrelated parameters for the Chicago excavations presented herein are E_{50}^{ref} and φ' (Calvello and Finno 2004). Results were also sensitive to changes in values of parameter *m*. However, parameter *m* was not included in the regression because the values of the correlation coefficients between parameters *m* and E_{50}^{ref} were very close to 1.0, indicating that the two parameters were not likely to be simultaneously and uniquely optimized. When values of φ' were kept constant at their initial estimates, and only the stiffness parameters, E_{50}^{ref}, were optimized, the calibrations of the simulations presented subsequently were successful. Finno and Calvello (2005) showed that shear stress levels in the soil around the excavation were much less than those corresponding to failure for the great majority of the soil. This indeed is expected for excavation support systems that are designed to restrict adjacent ground movements to acceptably small levels, and hence one would expect the stiffness parameters to have a greater effect on the simulated results than failure parameters. Furthermore, use of this model restricts one to the use of inclinometer data obtained close to a support wall because the model does not include the capability for handling small strain non-linearity.

Parameter Optimization at Early Stages of Excavation

The ability of the approach to provide optimized parameters at an early stage of excavation which leads to good predictions of subsequent performance is illustrated by the Chicago Ave. and State St. subway renovation project in Chicago (Finno et al. 2002). This project involved the excavation of 12.2 m of soft to medium clay within 2 m of a school supported on shallow foundations. Figure 9 shows a section of the excavation support system and the subsurface conditions. The support system consisted of a secant pile wall with three levels of support, which included pipe struts (1st level) and tieback anchors (2nd and 3rd levels). The subsurface conditions consisted of an urban fill, mostly medium dense sand but also containing construction debris, overlying four strata associated with the advance and retreat of the Wisconsin-aged glacier. The upper three are ice margin deposits deposited underwater, and are distinguished by water content and undrained shear strength (Chung and Finno, 1992). With the exception of a clay crust in the upper layer, these deposits are lightly overconsolidated as a

result of lowered groundwater levels after deposition and/or aging. Stratigraphy is shown in terms of Chicago City Datum (CCD) elevation.

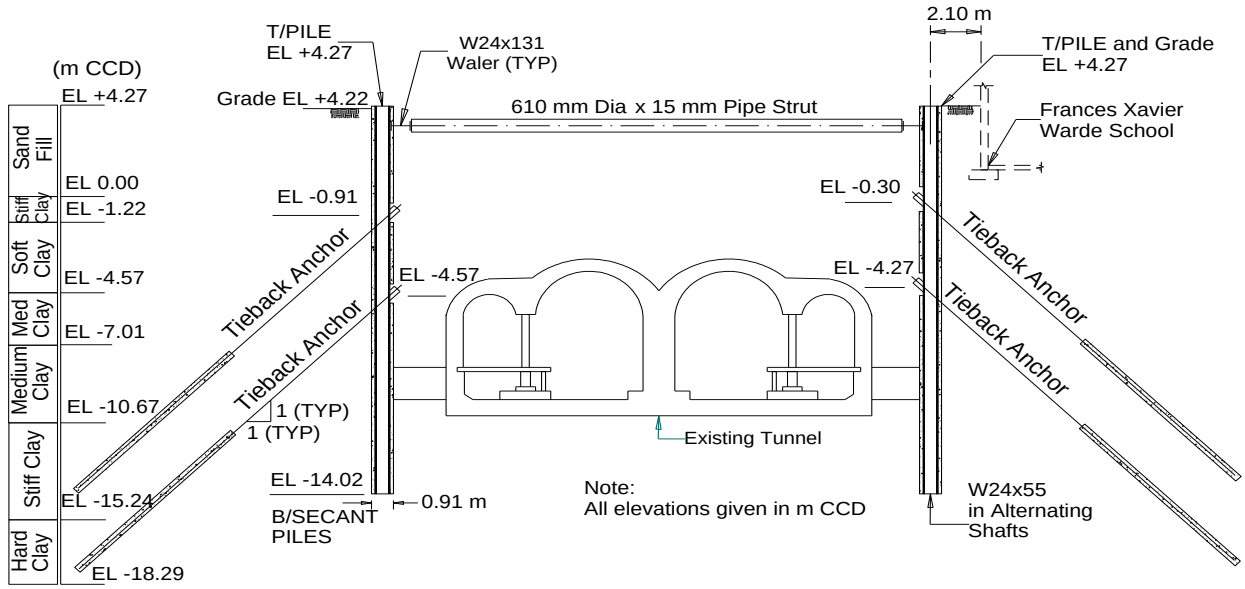

Figure 9. Support system for Chicago-State excavation (Finno et al. 2002)

A complete record of performance of the excavation can be found in Finno et al. (2002). Figure 10 summarizes deformation responses to excavation and support. Both lateral movements and settlements are shown, although optimization was based solely on the former. The movements that occurred as the secant pile wall extend through all compressible layers. This is important when using these observations to calibrate parameters using inverse techniques in that these movements occur at an early stage of the excavation. These observations were sufficient to optimize parameters in all layers so that movements could be "predicted" at subsequent stages of excavation. It is important to realize that the H-S model used for this analysis did not include effects of small strain non-linearity and hence relatively large movements were needed before any adjustments could be made to the model parameters.

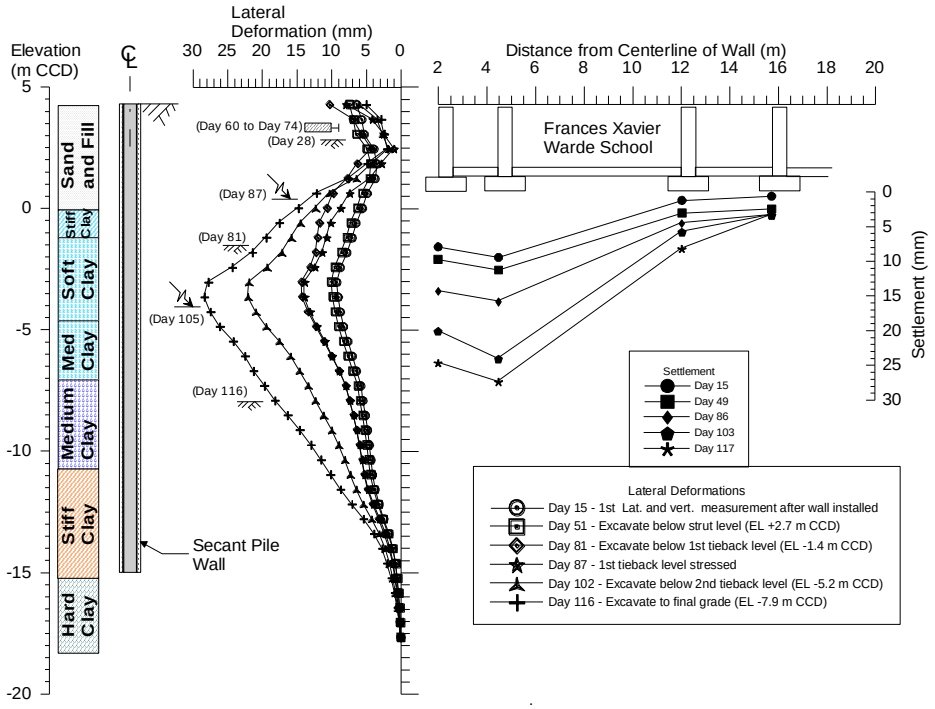

Figure 10. Lateral movements and settlements at Chicago-State excavation (Finno et al. 2002)

Very little movement beyond that which occurred during wall installation were observed until the excavation was lowered below EL. –1.4 m CCD; a maximum of 4 mm additional lateral movement occurred as a result of excavating to this elevation. This behavior suggests that the upper clays initially are relatively stiff, and provide field indications of the small strain nonlinearity of these soils. The secant pile wall incrementally moved toward the excavation in response to excavation-induced stress relief. When the excavation reached final grade, the maximum lateral movement was 28 mm. The school settled as the secant pile wall moved laterally. The maximum settlement at the school at the end of excavation also was 28 mm when the excavation bottomed out.

Table 3 shows the calculation phases and the construction stages used in the finite element simulations. Note that the tunnel tubes and the school adjacent to the excavation were explicitly modeled in the first 12 phases of the simulation to take into account the effect of their construction on the soil surrounding the excavation. Stages 1, 2, 3, 4 and 5 in the optimization process refer to the construction stages for which the computed results were compared to inclinometer data taken from two inclinometers on opposite sides of the excavation. Construction steps not noted as "consolidation" on Table 3 were modeled as undrained. Consolidation stages were included after the tunnel, school and wall installation calculation phases to permit excess pore water pressures to equilibrate. Details about the definition of the finite element problem, the calculation phases and the model parameters used in the simulation can be found in Calvello (2002).

Table 3. FE simulation of construction

Phase	Construction step	Simulation stage
0	Initial conditions	
1-4 5	Tunnel construction (1940) Consolidation	
6-10 11-12	School construction (1960) Consolidation	
13	Drill secant pile wall (1999)	
14	Place concrete in wall	Stage 1
15	Consolidation (20 days)	
16	Excavate and install struts	Stage 2
17	Excavate below first tieback level	
18	Prestress first level of tiebacks	Stage 3
19	Excavate below second tieback level	
20	Prestress second level of tiebacks	Stage 4
21	Excavate to final grade	Stage 5

Visual examination of the horizontal displacement distributions at the inclinometer locations provides the simplest way to evaluate the fit between computed and measured field response. When computations were made based on parameters derived from results of drained triaxial tests, the finite element model computed significantly larger displacements at every construction stage (Finno and Calvello 2005). The maximum computed horizontal displacements were about two times the measured ones and the computed displacement profiles result in significant and unrealistic movements in the lower clay layers. As one would expect, these results indicated that the stiffness properties for the clay layers based on conventionally-derived triaxial data were less than field values.

Figure 11 shows the comparison between the measured field data from both sides of the excavation and the computed horizontal displacements when parameters are optimized based on stage 1 observations. The improvement of the fit between the computed and measured response is significant. Despite the fact that the optimized set of parameters is calculated using only stage 1 observations, the positive influence on the calculated response is substantial for all construction stages. At the end of the construction (i.e. stage 5) the maximum computed displacement exceeds the measured data by only about 15%. These results are significant in that a successful recalibration of the model at an early construction stage positively affects subsequent "predictions" of the soil behavior throughout construction.

Analyses also were made wherein parameters were recalibrated at every stage until the final construction stage (stage 5). At every new construction stage, the inclinometer data relative to that stage were added to the observations already available. Results indicated that difference between the fit shown in Figure 11 and with those calibrated after every increment was not significant. In essence, the inverse analysis performed after the first construction stage "recalibrated" the model parameters in such a way that the main behavior of the soil layers could be accurately "predicted" throughout construction.

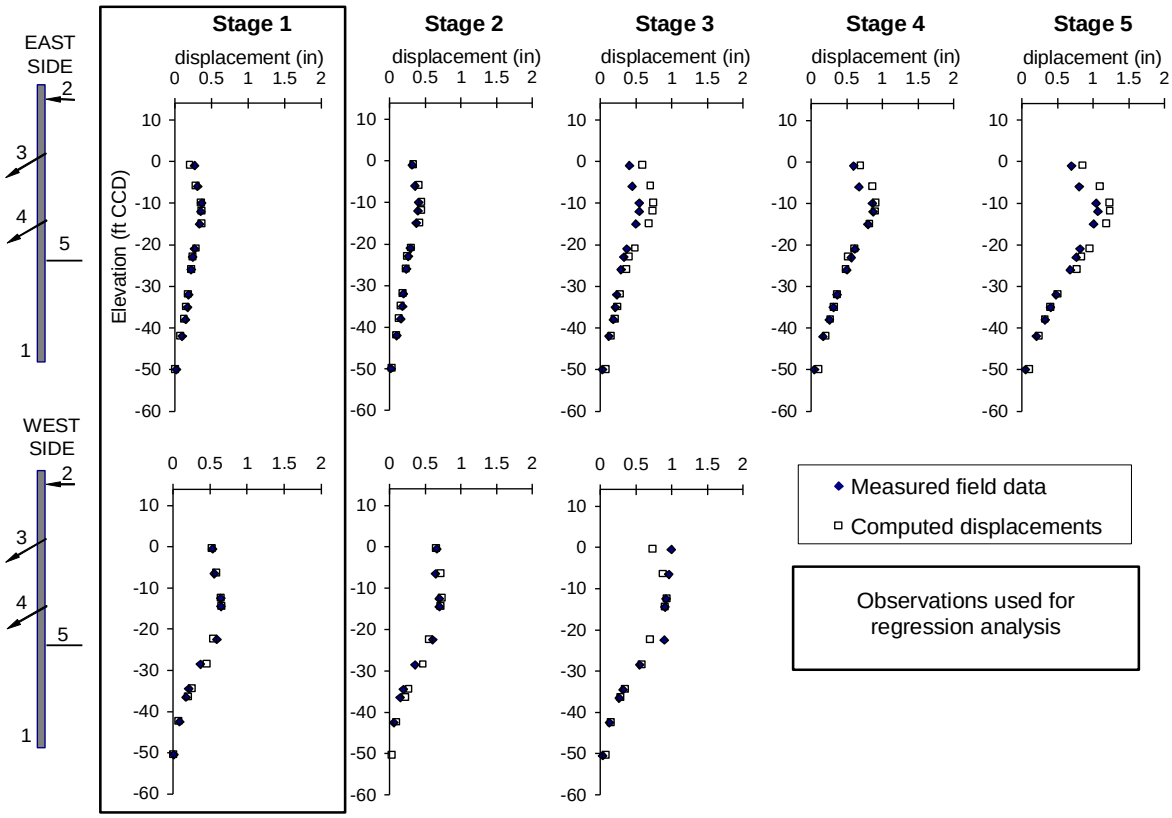

Figure 11. Comparison of observed and computed horizontal displacements (after Finno and Calvello 2005)

Applicability of Optimized Parameters in Similar Geology

To show the applicability of the optimized parameters that formed the basis of the good agreement in Figure 11 to other excavation sites in these soil deposits, the results of numerical simulations are presented in Figures 12 and 13 based on these optimized parameters for the conditions at the Lurie (Finno and Roboski 2005) and the Ford Design Center (Blackburn and Finno 2007) excavations, respectively. The geologic origin of the most compressible material is similar for all three cases, but the sites are located as much as 15 km apart. Consequently one should expect some variability in the actual parameters at each site.

Examining the comparisons in the clay layers below EL. –5 m CCD for the Lurie data on Figure 12, reasonable agreement is observed at stages 5 and 6, with significant differences seen at stage 4. This is likely caused by the fact that the H-S model used herein does not include provisions to represent the large stiffness degradation with small strains. As discussed previously, one must select moduli that represent the average strains within the soil mass, and when the movements are small, the average modulus should be higher in a model that does not consider the small strain modulus degradation. As noted, the agreement between computed and observed responses was good for the latter stages of excavation where the lateral movements were larger.

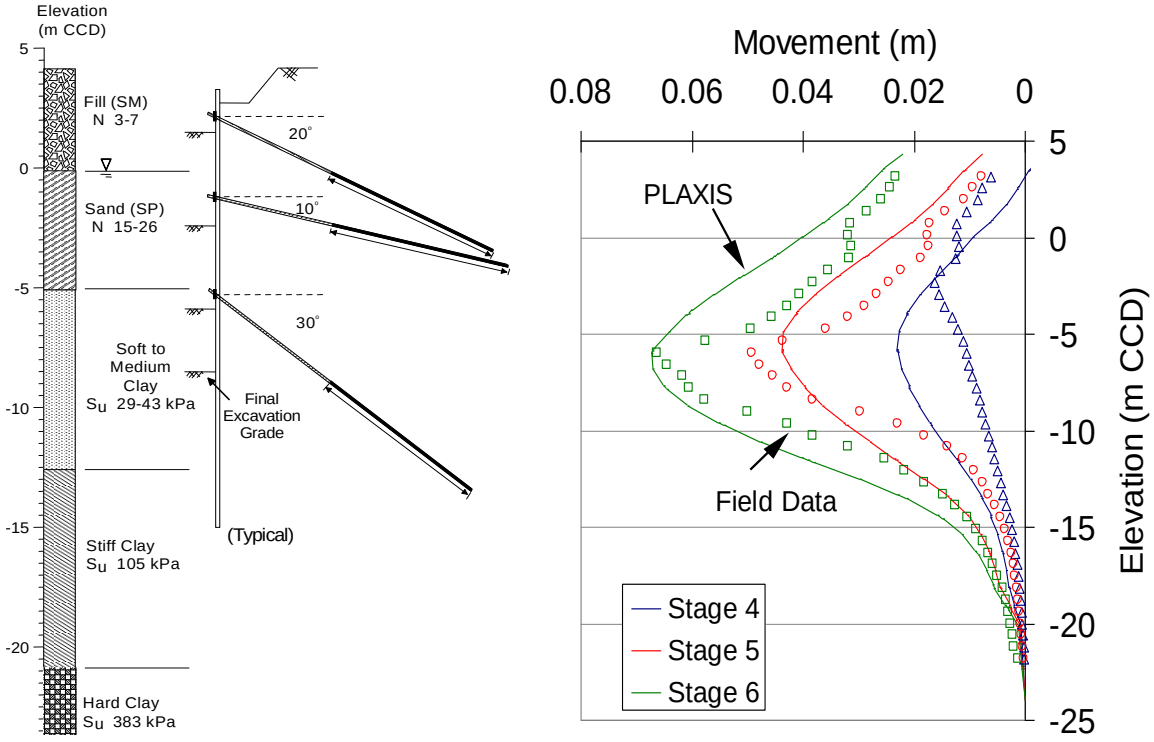

Figure 12. Computed and observed lateral movements: Lurie excavation with optimized parameters from Chicago-State excavation

At the Ford Center, the numerical results shown in Figure 13 followed similar trends as the observed data, but with larger magnitudes. The parameters used in the analysis again were based on the larger deformations that were present at the Chicago-State site, and hence resulted in larger deformations than were observed at the Ford Center. In any case, the application of the Chicago-State based optimized parameters to both the Lurie and Ford sites resulted in reasonable agreement with the observed lateral movements, within the limitations of the analyses. Application of the inverse techniques to these data resulted in improved fit with minor changes to the parameters (Rechea 2006).

CONCLUDING REMARKS

This paper describes an adaptive management approach to control ground movements caused by making a deep supported excavation. Successful applications of this approach depend equally on reasonable numerical simulations of performance, the type of monitoring data used as observations, and the inverse analysis techniques used to minimize the difference between predictions and observed performance.

The calibration by inverse analysis of the various simulations presented herein indicated that the numerical methodology developed to optimize a finite element model of an excavation can be very effective in minimizing the errors between the measured and computed results. However, the convergence of an inverse analysis to an "optimal solution" (i.e. best-fit between computed results and observations) does not necessarily mean that the simulation is satisfactorily calibrated. A geotechnical evaluation of the optimized parameters is always necessary to verify

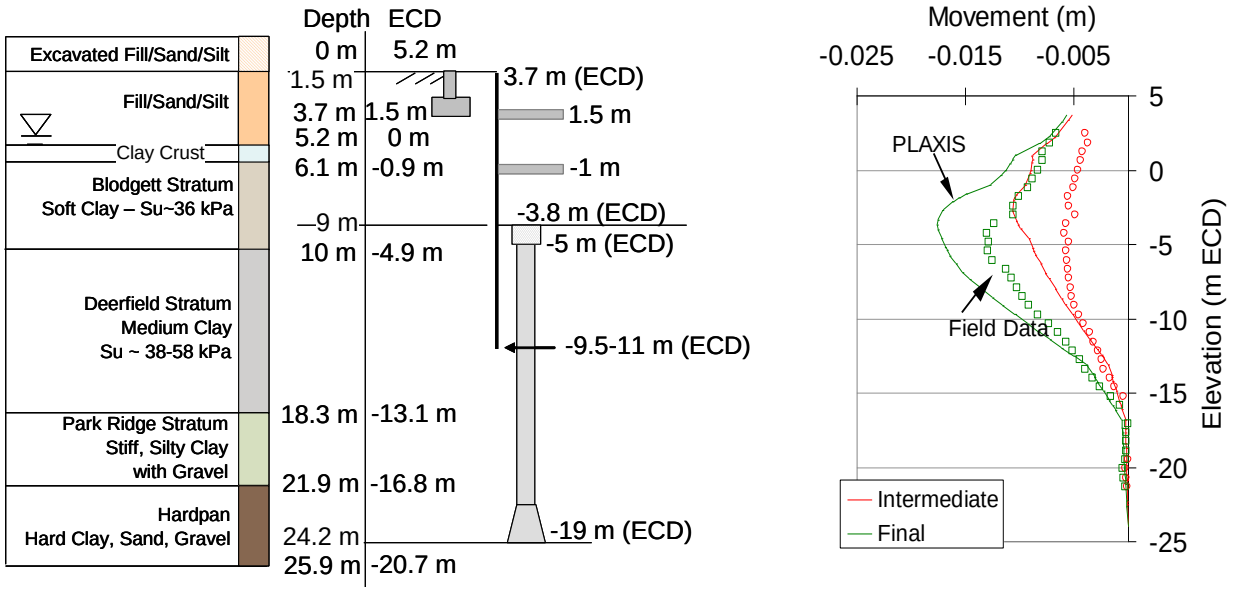

Figure 13. Computed and observed lateral movements at Ford excavation based on optimized parameters from Chicago-State excavation

the reliability of the solution. For a model to be considered "reliably" calibrated both the fit between computed and observed results must be satisfactory (i.e. errors are within desired and/or accepted accuracy) and the best-fit values of the model parameters must be reasonable. See Finno and Calvello (2005) for such an evaluation for the parameters obtained from the Chicago-State performance data.

The key to the successful calibration of an excavation lies in defining a "well posed" inverse analysis problem to calibrate the simulation. The parameters optimized by inverse analysis are few compared to the total number of parameters defining the behavior of the simulation. Indeed, the majority of the input parameters is estimated by conventional means and never "re-calibrated." Yet, the optimization can be effective if a finite element simulation of the excavation adequately reproduces the stress history of the soil on site and the soil model adequately represented the behavior of the clays, at least in terms of appropriate field observations.

The adaptive management approach in its current state is subjected to limitations. Real time collection of data is limited to that obtained by robotic total stations and relatively expensive versions of in-place inclinometers. At the time of this writing, commercial finite element codes do not include verified constitutive models that can represent small strain non-linearity. On-going work at Northwestern related to excavation support includes evaluating the relationship among the small strain non-linearity of very stiff layers into which the toe of diaphragm walls are embedded and the non-linear response of the diaphragm wall itself.

ACKNOWLEDGEMENTS

This work would not have been possible without the many contributions of former graduate students and post-doctoral scholars at Northwestern University who worked on developing the inverse analysis methods, collecting detailed field performance data, and conducting careful laboratory experiments, including Michele Calvello, Cecilia Rechea, Sebastian Bryson, Jill Roboski, Tanner Blackburn, Terry Holman, Wan Jei Cho, Greg Andrianis, Miltos Langousis, Young-Hoon Jung, Taesik Kim and Fernando Sarabia. Financial support for

this work was provided by National Science Foundation grant CMS-0219123 and the Infrastructure Technology Institute (ITI) of Northwestern University. The support of Dr. Richard Fragaszy, program director at NSF, is greatly appreciated.

REFERENCES

Blackburn, J.T., Sylvester, K. and Finno, R.J. (2005). "Observed bracing responses at the Ford Design Center excavation," *Proceedings, 16th International Conference on Soil Mechanics and Geotechnical Engineering*," Japan, Vol. 3, 1443-1446.

Blackburn, J.T. and Finno, R.J., (2007). "Three-Dimensional Responses Observed in an Internally Braced Excavation in Soft Clay," *Journal of Geotechnical and Geoenvironmental Engineering*, ASCE, 133 (11), 1364-1373.

Boone, S. J. (1996). "Ground-movement-related building damage," *Journal of Geotechnical and Geoenvironmental Engineering*, ASCE, 122(11), 886-896.

Boscardin, M.D. and Cording, E.J. (1989). "Building response to excavation-induced settlement*," Journal of Geotechnical and Geoenvironmental Engineering*, ASCE, 115(1), 1-21.

Burland, J. B., and Wroth, C. P. (1975). "Settlement of buildings and associated damage," *Proc. Conference on Settlement of Structures*, Cambridge, 611-654.

Burland, J.B. (1989). "'Small is beautiful' – the stiffness of soils at small strains: Ninth Laurits Bjerrum Memorial Lecture." *Canadian Geotechnical Journal*, Vol. 26, 499-516.

Calisto, L. and Calebresi, G. (1998). "Mechanical behavior of a natural soft clay." *Geotechnique*, Vol. 48 (4), 495-513.

Calvello, M. (2002). "Inverse Analysis of a Supported Excavation through Chicago Glacial Clays," PhD thesis, Northwestern University, Evanston, IL.

Calvello M. and Finno R.J. (2002). "Calibration of soil models by inverse analysis." *Proc. International Symposium on Numerical Models in Geomechanics, NUMOG VIII*, Balkema, p. 107-116.

Calvello M. and Finno R.J. (2003). "Modeling excavations in urban areas: effects of past activities." *Italian Geotechnical Journal*, 37(4), 9-23.

Calvello M. and Finno R.J. (2004). "Selecting parameters to optimize in model calibration by inverse analysis." *Computers and Geotechnics*, Elsevier, Vol. 31, 5, 2004, 411-425.

Chung, C.-K. and Finno, R.J. (1992). "Influence of Depositional Processes on the Geotechnical Parameters of Chicago Glacial Clays," *Engineering Geology*, 32, 225-242.

Cho, W.J. (2007). "Recent stress history effects on compressible Chicago glacial clay," PhD thesis, Northwestern University, Evanston, IL.

Cho, W.J. and Finno, R.J. (2010). "Stress-Strain Response of Block Samples of Compressible Chicago Glacial Clays," *Journal of Geotechnical and Geoenvironmental Engineering*, ASCE, Vol. 136, No. 1, 178-188.

Clayton, C.R.I., and Heymann, G. (2001). "Stiffness of geomaterials at very small strains." *Geotechnique*, Vol. 51 (3), 245-255.

Clough, G.W. and Mana, A.I. (1976). "Lessons learned in finite element analysis of temporary excavations." *Proceedings, 2nd International Conference on Numerical Methods in Geomechanics*, ASCE, Vol. I, 496-510.

Clough, G. W., Smith, E.M., and Sweeney, B.P. (1989). "Movement control of excavation support systems by iterative design." *Current Principles and Practices, Foundation Engineering Congress*, Vol. 2, ASCE, 869-884.

Finno, R.J. (2007). "Use of monitoring data to update performance predictions of supported excavations," theme lecture in the Proceedings, *FMGM 2007, International Symposium on Field Measurements in Geomechanics*, ASCE, Boston, September.

Finno, R.J., Atmatzidis, D.K., and Nerby, S.M. (1988). "Ground response to sheet-pile installation in clay," *Proceedings, Second International Conference on Case Histories in Geotechnical Engineering*, St. Louis, MO.

Finno, R.J. and Blackburn, J.T. (2005). "Automated monitoring of supported excavations," *Proceedings, 13th Great Lakes Geotechnical and Geoenvironmental Conference, Geotechnical Applications for Transportation Infrastructure,* GPP 3, ASCE, Milwaukee, WI., 1-12.

Finno R.J., Bryson L.S. and Calvello M. (2002). "Performance of a stiff support system in soft clay." *Journal of Geotechnical and Geoenvironmental Engineering*, ASCE, Vol. 128, No. 8, p. 660-671.

Finno, R.J. and Calvello, M. (2005). "Supported excavations: the observational method and inverse modeling." *Journal of Geotechnical and Geoenvironmental Engineering*. ASCE, 131 (7).

Finno, R.J. and Roboski, J.F., (2005). "Three-dimensional Responses of a Tied-back Excavation through Clay," *Journal of Geotechnical and Geoenvironmental Engineering*, ASCE, Vol. 131, No. 3, 273-282.

Finno, R.J. and Tu, X. (2006). "Selected Topics in Numerical Simulation of Supported Excavations," *Numerical Modeling of Construction Processes in Geotechnical Engineering for Urban Environment,* International Conference of Construction Processes in Geotechnical Engineering for Urban Environment, Th. Triantafyllidis, ed., Bochum, Germany, Taylor & Francis, London, 3-20.

Finno, R.J., Voss. F.T., Jr., Rossow, E., and Blackburn, J.T. (2005). "Evaluating damage potential in buildings affected by excavations," *Journal of Geotechnical and Geoenvironmental Engineering*, ASCE,131(10), 1119-2100.

Finno, R.J., Blackburn, J.T. and Roboski, J.F., (2007). "Three-dimensional Effects for Supported Excavations in Clay," *Journal of Geotechnical and Geoenvironmental Engineering*, ASCE, Vol. 133, No. 1, January, 30-36.

Geddes, J.D. (1977). "Construction in areas of large ground movements." *Proc., Conf. on Large Ground Movements and Structures*, Halstead Press, New York, NY 623-646.

Geddes, J.D. (1991). Discussion of "Building response to excavation-induced settlement," by Boscardin, M.D. and Cording, E.J., *Journal of Geotechnical and Geoenvironmental Engineering*, ASCE, 117(8), 1276-1278.

Ghaboussi, J. and Pecknold, D.A. (1985). "Incremental finite element analysis of geometrically altered structures." *International Journal of Numerical Methods in Engineering*. Vol 20(11) 2061-2064.

Hashash, Y.M.A., and A.J. Whittle (1996) "Ground movement prediction for deep excavations in soft clay," *Journal of Geotechnical Engineering*, Vol. 122, No. 6, 474-486.

Hashash, Y. M. A., Marulanda, C. Ghaboussi, J. and Jung, S. (2006) "Novel approach to integration of numerical modeling and field observations for deep excavations," *Journal of Geotechnical and Geoenvironmental Engineering*, Vol. 132, No. 8, 1019 - 1031.

Hill, M. (1998). "Methods and guidelines for effective model calibration." *U.S. Geological Survey. Water-resources investigations report 98-4005*.

Holman, T.P. (2005). "Small strain behavior of compressible Chicago glacial clay." PhD thesis, Northwestern University, Evanston, IL.

Jardine, R.J., Symes, M.J. and Burland, J.B. (1984). "The measurement of small strain stiffness in the triaxial apparatus." *Geotechnique*, Vol. 34 (3), 323-340.

Koutsoftas, D. C., P. Frobenius, C.L Wu, D. Meyersohn, and R. Kulesza (2000). "Deformations during cut-and-cover construction of Muni Metro Turnback project," *Journal of Geotechnical and Geoenvironmental Engineering*, Vol. 126, No. 4, 344-359.

Langousis, M.. (2007). "Automated Monitoring and Inverse Analysis of a Deep Excavation in Seattle," MS thesis, Northwestern University, Evanston, IL.

Ledesma, A., Gens, A, and Alonso, E.E. (1996). "Estimation of parameters in geotechnical backanalysis. I – Maximum likelihood approach," *Computers and Geotechnics,* Vol. 18, No. 1, 1-27.

O'Rourke, T.D. and Clough, G.W. (1990). "Construction induced movements of insitu walls." *Proceedings, Design and Performance of Earth Retaining Structures,* Lambe, P.C. and Hansen L.A. (eds). ASCE, 439-470.

O'Rourke, T.D. and O'Donnell, C.J. (1997). "Deep rotational stability of tiedback excavations in clay," *Journal of Geotechnical Engineering*, ASCE, Vol. 123(6), 506-515.

Ou, C.Y., Chiou, D.C. and Wu, T.S. (1996). "Three-dimensional finite element analysis of deep excavations." *Journal of Geotechnical Engineering*, ASCE, 122(5), 473-483.

Ou C.Y., Tang Y.G. (1994). "Soil parameter determination for deep excavation analysis by optimization." *Journal of the Chinese Institute of Engineering*, Vol. 17(5)}, pp.671-688

Peck R.B. (1969). "Deep excavations and tunneling in soft ground." *Proceedings, 7th International Conference of Soil mechanics and Foundation Engineering, State-of-the-ArtVolume*, 225-290.

Poeter EP and Hill M.C. (1997). "Inverse Methods: A Necessary Next Step in Groundwater Modeling," *Ground Water*, Vol. 35, no. 2, 250-260.

Poeter E.P. and Hill M.C. (1998). "Documentation of UCODE, a computer code for universal inverse modeling." *U.S. Geological Survey Water-Resources investigations report 98-4080,* 116 pp.

Rechea, C. (2006). "Inverse analysis of excavations in urban environments," PhD thesis, Northwestern University, Evanston, IL.

Santagata, M., Germaine, J.T. and Ladd, C.C. (2005). "Factors Affecting the Initial Stiffness of Cohesive Soils." *Journal of Geotechnical and Geoenvironmental Engineering*, ASCE, Vol. 131(4), 430-441.

Sabatini, P.J. (1991). "Sheet-pile installation effects on computed ground response for braced excavations in soft to medium clays." MS thesis, Northwestern University, Evanston, IL.

Schantz, T., Vermeer, P.A. and Bonnier, P.G. 1999. "Formulation and verification of the Hardening–Soil Model." *R.B.J. Brinkgreve, Beyond 2000 in Computational Geotechnics.* Balkema, Rotterdam, 281-290.

Skempton, A.W. and MacDonald, D.H. (1956). "The allowable settlements of buildings," *Proc. Institution Civil Engrs.*, London, England, Part 3, Vol. 6, 727-768.

Stallebrass, S.E. and Taylor, R.N. (1997). "The development and evaluation of a constitutive model for the prediction of ground movements in overconsolidated clay." *Geotechnique*, Vol. 47 (2) 235-253.

Su, Y.Y., Hashash, Y.M.A. and Liu, L.Y. (2006). "Integration of construction as-built data with geotechnical monitoring of urban excavation," *Journal of Construction Engineering and Management*, Vol. 132, No. 12, 1234-1241.

Son, M. and Cording, E.J. (2005). "Estimation of building damage due to excavation–induced ground movements," *Journal of Geotechnical and Geoenvironmental Engineering*, ASCE, 131(2), 162-177.

Trupp, T., Marulanda, C., Hashash, Y.M.A., Liu, L., and Ghaboussi, J., (2004). "Novel methodologies for tracking construction progress of deep excavations," *Geo-Trans 2004*, ASCE, Los Angeles, CA.

Tu, X.X. (2007). "Tangent stiffness model for clays including small strain non-linearity." PhD thesis, Northwestern University, Evanston, IL.

Viggiani, G. and Tamagnini, C. (1999). "Hypoplasticity for modeling soil non-linearity in excavation problems." *Pre-failure Deformation Characteristics of Geomaterials*, M. Jamiolkowski, M, Lancellotta, R. and Lo Presti, D. (eds.), Balkema, Rotterdam, 581-588.

Whittle, A.J. and Kavvadas, M.J. (1994). "Formulation of MIT-E3 constitutive model for overconsolidated clays." *Journal of Geotechnical and Geoenvironmental Engineering*, ASCE, Vol. 120(1), 173-198.

Whittle, A.J., Y.M.A. Hashash, and R.V. Whitman (1993). "Analysis of deep excavation in Boston," *Journal of Geotechnical Engineering*, Vol. 119, No. 1, 69-90.